Proceedings of the 4th International Conference on Functional Materials and Civil Engineering
DOI: 10.54254/2755-2721/2026.36441

Preparation Strategies of MXene Materials: From Chemical Etching to Al-Assisted A-Site Extraction

Chengzong Shen

School of Materials Science and Engineering, Southeast University, Nanjing, China
213230471@seu.edu.cn

Abstract. With high electrical conductivity and tunable surface chemistry, MXenes, a class of two-dimensional transition metal carbides, nitrides, and carbonitrides, have been employed in energy storage, electromagnetic interference shielding, and catalysis. However, synthesis routes strongly influence their structural features, surface terminations, and functional properties, and the effects of different preparation strategies have not been fully clarified. Accordingly, this paper compares six major MXene preparation strategies, including HF etching, LiF/HCl in situ etching, alkali-hydrothermal synthesis, electrochemical exfoliation, Lewis acid molten salt etching, and bottom-up direct growth, by linking etchant chemistry with surface termination evolution and defect formation. The effects of these strategies on yield, flake size, electrical conductivity, and dominant defect types are systematically analyzed. In addition, an Al-assisted solid-state A-site extraction route for Ti_2SnC is evaluated through experimental evidence of thermally driven Sn extraction into Al substrates at 650 °C and spontaneous Sn whisker growth. The comparison shows that etchant-induced defects limit top-down MXene synthesis, whereas fluoride-free routes enable diverse surface terminations. Moreover, solid-state A-site extraction provides an alternative to conventional chemical etching.

Keywords: MXenes, MAX phases, Synthesis strategies, Fluoride-free synthesis, Surface terminations

1. Introduction

Following their discovery in 2011, MXenes, a class of two-dimensional transition metal carbides, nitrides, and carbonitrides ($M_{n+1}X_nT_x$), have drawn considerable interest owing to their outstanding electrical conductivity, hydrophilic surface characteristics, and superior mechanical strength [1, 2]. They have also shown strong promise for applications in energy storage, electromagnetic interference shielding, catalysis, and biosensing [3, 4]. MXenes are typically obtained by selectively etching the A layer from MAX phases, with their composition primarily determined by the MAX precursor. In contrast, surface terminations, defect structures, flake size, and interlayer spacing strongly depend on the etching system and reaction conditions [4-6]. Despite the continuous expansion of synthesis routes in recent years and a gradual transition toward fluoride-free or low-fluoride systems, a coherent mechanistic framework for comparing different

© 2026 The Authors. This is an open access article distributed under the terms of the Creative Commons Attribution License 4.0 (https://creativecommons.org/licenses/by/4.0/).

DOI: 10.54254/2755-2721/2026.36441

preparation strategies remains absent. In particular, the synergistic effects of etchant chemistry, reaction conditions, and post-treatment processes on MXene structural evolution and property tuning have not yet been systematically quantified [7-9]. This study compares six MXene synthesis routes based on the formation mechanisms, including hydrofluoric acid (HF) etching, lithium fluoride/hydrochloric acid (LiF/HCl) etching, fluoride-free alkaline hydrothermal etching, electrochemical delamination (ED), Lewis acidic molten salt etching, and bottom-up synthesis. The effects of these routes on yield, flake size, electrical conductivity, surface termination chemistry, defect characteristics, and scalability are evaluated. Besides, an Al-assisted solid-state A-site extraction strategy for Ti_2SnC synthesis is analyzed based on reported Sn whisker growth and thermally driven Sn migration from Al substrates [10]. These analyses highlight the role of synthesis design in controlling MXene structures and properties.

2. Fundamental principles of MXene synthesis

2.1. MAX phase structure and A-site removal

MAX phases crystallize in hexagonal $P6_3/mmc$ symmetry, consisting of M-X slabs interleaved with atomically thin A-atom layers. Both experimental measurements and DFT calculations indicate that M-A bonds are systematically weaker than the covalent M–X intralayer bonds across the MAX phase family, although the strength difference depends sensitively on the A-element identity [11]. And this intrinsic bonding hierarchy provides the fundamental driving force for selective A-site removal.

In practice, the removal behavior strongly depends on the chemical nature of the A element. Al-containing MAX phases exhibit relatively strong M-A interactions and therefore require aggressive etching conditions, whereas Sn- and Ga-based systems enable milder extraction pathways. For HF-based routes, A-site removal cannot be attributed solely to Al-F bond formation (~−670 kJ/mol). Instead, it proceeds via an oxidation–coordination synergistic mechanism, in which fluoride ions first oxidize surface Al atoms and the resulting Al^{3+} species are stabilized through coordination with excess F^- to form soluble AlF_4^- / AlF_6^{3-} complexes. The differences in fluoride complex stability among non-Al A elements (Si, Ga, Sn, In, Pb) lead to distinct etching behaviors, requiring extraction chemistries beyond conventional fluoride-based approaches [4, 12].

2.2. MXene formation: etching to delamination process

MXene formation proceeds through three sequential and interdependent stages governed by distinct physical and chemical driving forces. Initially, the process begins with etching, in which the A-atom layer is selectively removed from the MAX phase precursor, resulting in a loosely stacked multilayer structure stabilized by residual van der Waals and hydrogen-bonding interactions. Then, intercalation occurs through the insertion of guest species, typically Li^+, tetrabutylammonium (TBA^+), or dimethyl sulfoxide (DMSO), into the interlayer galleries. This step increases the interlayer spacing from approximately 20 Å to 30–45 Å, primarily via electrostatic shielding of negatively charged MXene sheets and solvation-induced swelling from co-intercalated molecules. In addition, delamination is achieved through mild mechanical agitation, such as sonication or shaking, which breaks weakened interflake interactions to yield single- or few-layer nanosheets. As each stage is governed by relatively independent parameters, etching, intercalation, and delamination conditions can be independently tuned to optimize MXene morphology and properties.

DOI: 10.54254/2755-2721/2026.36441

2.3. The surface termination formation and control

Following A-layer removal, the exposed M surfaces become coordinatively unsaturated and reactive, promoting spontaneous adsorption of surface species from the surrounding environment. As a result, surface termination chemistry is not intrinsic but is strongly dictated by the reaction medium. In aqueous HF-containing systems, the coexisting species including F^-, OH^-, and H_2O generate mixed terminations of –F, –OH, and –O, whose relative distribution is governed by pH, fluoride concentration, and temperature. In contrast, halide-rich molten salt environments favor –Cl, –Br, or –I terminations due to the high halide activity in the melt. For alkali-hydrothermal routes, fluoride-free basic conditions predominantly produce –O and –OH terminated surfaces. In general, heterogeneous termination distributions generated in wet-chemical processes hinder the establishment of clear structure-property correlations. This limitation drives the development of precise surface termination control strategies for advanced MXene synthesis [13].

3. MXene synthesis pathways from wet chemical etching to bottom-up growth

3.1. The solution-based top-down etching of MAX phases

In solution-based top-down etching, selective removal of A-site elements from MAX phases enables MXene formation, while etching conditions, intercalation behavior, and charge regulation collectively influence surface terminations, flake morphology, and structural integrity.

The earliest and most widely used route is direct etching of Ti_3AlC_2 with concentrated HF (10–50 wt%) at room temperature [1]. While effective for A-layer removal, low HF concentrations lead to incomplete etching, whereas higher concentrations (≥40 wt%) induce non-selective Ti dissolution at defect sites, resulting in "Swiss-cheese" morphologies and mixed surface terminations dominated by –F (30–60 at%) and –OH groups [5]. To improve control and product quality, the LiF/HCl system developed by Ghidiu et al. enables in situ HF generation and simultaneous Li^+ intercalation, expanding interlayer spacing and facilitating delamination to yield larger flakes (1–5 μm vs. 0.5–2 μm) with reduced defects, a process known as the "MILD" method [5]. Delamination is typically achieved using organic bases (e.g., TBAOH, TMAOH) or cation-exchange strategies [5, 7]. Beyond fluoride-based routes, a fluoride-free alkaline hydrothermal method using concentrated NaOH (27.5 M, 270 °C) has also been reported, where Al is removed via $Al(OH)_4^-$ formation to produce predominantly –OH/–O-terminated $Ti_3C_2T_x$, though harsh conditions promote partial oxidation to TiO_2 and limit flake size (100 nm–1 μm) despite high yields (~90%) [7].

In contrast, electrochemical strategies introduce an external potential as an additional driving force for A-site removal. Yang et al. demonstrated selective Al extraction from Ti_3AlC_2 via anodic oxidation under potentiostatic control in aqueous electrolytes [8]. More recently, pulsed electrochemical exfoliation has further increased flake sizes up to 18.6 μm with over 90% mono- and bilayer yield. Nevertheless, challenges remain in achieving uniform large-area etching and complete delamination.

3.2. Redox-driven high-temperature etching in molten media

In molten media, MXene formation is governed by coupled redox reactions, in which A-site oxidation in MAX phases is driven by Lewis acid cations while the cations are simultaneously reduced. The feasibility of this process is determined by redox potential differences and Gibbs free energy criteria [9]. In the Lewis acid molten salt strategy introduced by Li et al., A-site elements are

DOI: 10.54254/2755-2721/2026.36441

selectively oxidized by molten metal halide cations, thus enabling their extraction through a coordinated redox process [9]. For example, a representative reaction is as follows:

$$Ti_3SiC_2+2CuCl_2\rightarrow Ti_3C_2+SiCl_4\uparrow+2Cu \quad (1)$$

Based on this mechanism, cation selection follows a thermodynamic requirement that the Lewis acid cation exhibits a higher redox potential than the target A-element, ensuring spontaneous oxidation and removal. Accordingly, $CuCl_2$, $ZnCl_2$, $CdCl_2$, $NiCl_2$, and $FeCl_2$ have been widely used at 450–750 °C for A-site extraction across diverse MAX phases. This molten salt route extends MXene synthesis beyond HF-based chemistry, enabling etching of chemically stable MAX phases such as Ti_3SiC_2 and Ti_3GaC_2 and thereby broadening accessible compositions. It also produces uniform –Cl terminations due to the high halide activity in the melt, while the relatively weak M–Cl bond enables subsequent post-synthetic exchange into –O, –NH, –S, –Se, –Br, and –Te terminations. Thus, more than 15 MXene compositions had been reported by 2023, with optimized yields exceeding 85% [14].

3.3. Bottom-up growth and direct MXene construction routes

By eliminating the need for MAX phase precursors, bottom-up growth and direct construction routes enable MXene synthesis via the assembly of M-X frameworks from elemental or simple compound sources under solid-state or vapor-phase conditions, thus extending the accessible compositional space beyond conventional top-down etching.

In this context, Wang et al. demonstrated that MXenes can be directly synthesized through solid-state reactions using elemental or simple compound precursors like Ti, $TiCl_4$, and C, forming Ti_2CCl_2 without the need for MAX phase intermediates [15]. This strategy enables access to compositions that are difficult to obtain through conventional A-site etching. The approach was subsequently extended to chemical vapor deposition (CVD), enabling the growth of vertically aligned MXene films on metal foil substrates. More recently, Wang et al. reported a vapor-phase route for MXene-like structures using CVD, although the phase purity and reproducibility remain unresolved [15]. For comparison, Table 1 summarizes representative MXene preparation methods by yield, morphology, and surface chemistry [15].

Table 1. Comparison of MXene preparation methods

Method	Conditions	Yield (%)	Flake size (μm)	Terminations	Key features
HF etching	HF (10–50 wt%), RT–50°C	60–93	0.5–2	–F, –OH, –O	High conductivity; severe defects
LiF/HCl (MILD)	35–45°C	88–91	1–5	–O, –OH, –F	Large flakes; moderate defects
Alkali-hydrothermal	200–270°C	90–92	0.1–1	–OH, –O	Fluoride-free; TiO_2 formation
Electrochemical	RT–60°C	40–50	0.5–18.6	–O, –Cl, –OH	Tunable; low yield
Lewis acid molten salt	450–750°C	78–85	2–10	–Cl	High crystallinity

DOI: 10.54254/2755-2721/2026.36441

Table 1. (continued)

CVD direct growth	600–1,100°C	Film	Continuous	–Cl, –Br	Bottom-up; non-powder

**Note: The 18.6 μm electrochemical flake size was reported in a single pulsed-exfoliation study and is not typical of electrochemical etching (0.5–2 μm). CVD-derived MXene conductivity lacks standardized values.

4. The structure-property relationships and solid-state A-site extraction in MXenes

4.1. Surface termination effects on electronic structure and stability

MXene properties are mainly governed by surface termination, controlling electronic structure, transport, and stability. In particular, surface terminations directly control the electronic structure of MXenes. –OH and –O terminations increase state localization and shift MXenes toward semimetallic or semiconducting behavior, while –F terminations lower the density of states near the Fermi level and suppress ion transport [13]. –Cl terminations (from molten-salt synthesis) retain higher conductivity and are more chemically exchangeable. Moreover, selective removal of –F terminations via vacuum annealing reduces electronic scattering and improves lithium-ion storage performance, showing that conductivity and electrochemical activity are strongly termination-dependent [3, 13].

In addition, surface terminations also determine oxidation pathways. For example, Ti-based MXenes oxidize in water via dissolved O_2, forming TiO_2, with oxidation rates strongly dependent on surface chemistry: –O-terminated surfaces are relatively stable, while –F and –OH accelerate degradation [16]. Importantly, these stability differences are primarily linked to surface reactivity rather than bulk structure. From a practical standpoint, stabilization strategies rely on limiting O_2exposure (e.g., Ar-purged storage and low temperature conditions) or reducing interfacial reactions using organic solvents and protective coatings [17].

4.2. Defect formation and evolution in different synthesis routes

MXene defect structures are primarily determined by the synthesis route, with each method producing a distinct and reproducible defect signature. Specifically, direct HF etching generates Ti vacancy defects that appear as through-thickness holes in SEM, resulting from non-selective dissolution of Ti at pre-existing lattice defects under highly aggressive conditions. In contrast, LiF/HCl (MILD) etching mainly introduces point defects, including residual Al sites (ICP-confirmed) and carbon vacancies (HAADF-STEM). Recent studies show that in-plane Ti and C vacancies dominate transport behavior, while edge defects are less critical; even ~0.3 at% Ti vacancies can measurably reduce conductivity [18]. Beyond acid etching routes, alkali-hydrothermal etching leads to partial oxidation, forming TiO_2 inclusions identified by anatase Raman peaks and Ti^{4+} XPS signals. Electrochemical etching causes edge over-etching and non-uniform delamination, reflected in AFM step-height variations. Molten-salt routes introduce metallic nanoparticles (Cu, Zn, Cd) from Lewis acid reduction, which can be removed by post-treatment. CVD synthesis instead yields intrinsic polycrystalline defects such as grain boundaries and stacking faults, observed by cross-sectional TEM. Notably, these defects also interact with post-synthesis instability. Ti-based MXenes oxidize in aqueous environments via dissolved O_2 to form TiO_2, and the rate depends on surface termination, with –O showing higher resistance than –F and –OH [13]. Besides, defect-rich regions further accelerate oxidation, making stability a coupled effect of structure and surface

DOI: 10.54254/2755-2721/2026.36441

chemistry. In practice, mitigation strategies include low-temperature Ar storage, organic solvent dispersion, and antioxidant coatings.

4.3. Solid-state A-site extraction through Al-assisted sink design

MXene-related synthesis can be extended beyond chemical etching through solid-state A-site extraction, where A-site atoms migrate under a chemical potential gradient instead of being removed by chemical dissolution. Within this framework, Ti_2SnC is used as a model system because Sn at the A-site shows high mobility. Sn exhibits weak M–Sn bonding, a low migration barrier (~0.66 eV), and long-range diffusion, as evidenced by spontaneous whisker formation and isotope tracing of lattice-origin transport [17]. Mechanochemical activation produces similar de-intercalation morphologies, whereas Ga alloying suppresses whisker growth, confirming the dependence of Sn extraction on A-site mobility [19, 20]. Sn release occurs above ~400 °C and increases near the Al melting temperature (660 °C). An Al sink promotes directional Sn extraction by establishing a chemical potential gradient. In Ti_2SnC/Al composites (1:0.1), annealing at 650 °C drives Sn migration into Al due to the low Sn solubility in Al (~0.003 at.%) and Al–Sn immiscibility (eutectic temperature: 228 °C). Sn diffusion into Al produces surface nanowires with diameters of 200–800 nm and lengths of several hundred micrometers (Figure 1) [10].

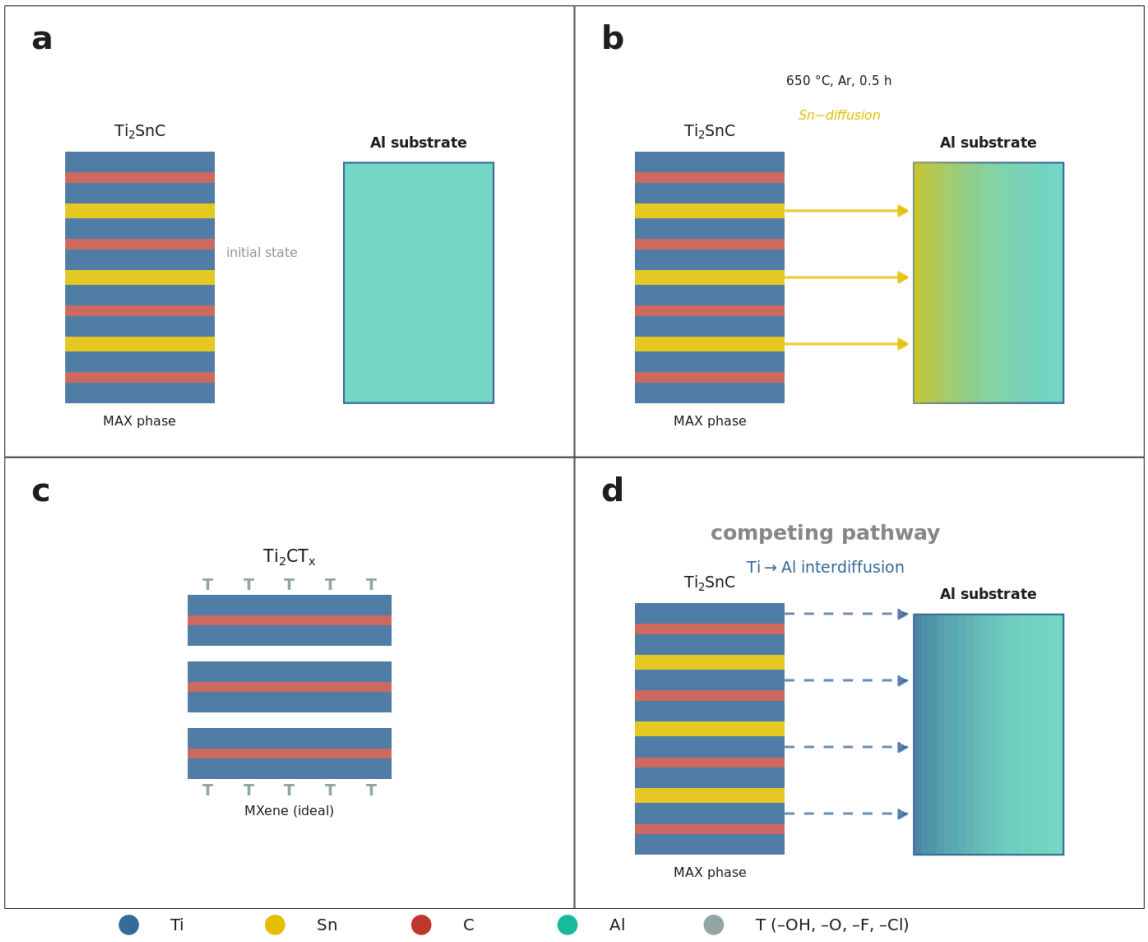

Figure 1. Al-assisted Sn extraction from Ti_2SnC: (a) initial state; (b) Sn diffusion into Al; (c) ideal MXene Ti_2CT_x structure; (d) competing Ti-Al interdiffusion pathway

DOI: 10.54254/2755-2721/2026.36441

The extraction process competes with interfacial reactions, including Ti–Al interdiffusion and $TiAl_3$ formation, which introduce kinetic constraints on A-site removal. DSC and XRD confirm concurrent Sn release, Al melting (600–673 °C), and formation of $TiAl_3$ and β-Sn phases, while the higher barrier for $TiAl_3$ formation (~3.1 eV) [21] indicates that interfacial compound formation can kinetically compete with A-site migration. More generally, DFT calculations across 211 MAX phases show that A-site migration barriers are generally below 1 eV (e.g., Cd 0.53 eV, In 0.63 eV, Ga 0.75 eV, Al ~0.83 eV), indicating that diffusion is not the rate-limiting step in most systems. Accordingly, extraction behavior is governed primarily by sink-induced thermodynamic driving force and interfacial selectivity rather than intrinsic diffusion kinetics. And this is supported by Ti_2InC/Al systems, where In nanowire formation occurs under analogous conditions [10].

5. Conclusion

This study explores MXene preparation strategies from conventional chemical etching to emerging solid-state A-site extraction, emphasizing the coupled nature of etching chemistry, surface termination, and defect formation across different synthesis routes. In addition, it further highlights a shift in the field from solution-based A-site removal toward sink-driven solid-state extraction enabled by intrinsic A-site mobility under chemical potential gradients. However, method comparison remains limited by inconsistent experimental conditions and the predominance of Ti-based systems. Solid-state extraction is further restricted by the poor control of competing A-site migration and interfacial compound formation. Key challenges include establishing standardized evaluation criteria, extending mechanistic understanding to diverse MAX chemistries, and improving kinetic selectivity through interface and sink engineering.

References

[1] Naguib, M., et al. (2011). Two-dimensional nanocrystals produced by exfoliation of Ti_3AlC_2. *Advanced Materials, 23*(37), 4248–4253.
[2] Naguib, M., et al. (2012). Two-dimensional transition metal carbides. *ACS Nano, 6*(2), 1322-1331.
[3] Li, Y., et al. (2020). A general Lewis acidic etching route for preparing MXenes with enhanced electrochemical performance. *Nature Communications, 11*, 1799.
[4] Huang, P., et al. (2023). Recent advances and perspectives of Lewis acidic etching routes. *ACS Nano, 17*(9), 4444-4468.
[5] Ghidiu, M., et al. (2014). Conductive two-dimensional titanium carbide "clay" with high volumetric capacitance. *Nature, 516*, 78-81.
[6] Alhabeb, M., et al. (2017). Guidelines for synthesis and processing of two-dimensional titanium carbide $Ti_3C_2T_x$ MXene. *Chemistry of Materials, 29*(18), 7633-7644.
[7] Li, T., et al. (2018). Fluorine-free synthesis of high-purity $Ti_3C_2T_x$ MXene via alkali treatment. *Angewandte Chemie International Edition, 57*(21), 6115–6119.
[8] Yang, S., et al. (2018). Fluoride-free synthesis of two-dimensional titanium carbide MXene using electrochemical etching. *Angewandte Chemie International Edition, 57*(43), 14361–14365.
[9] Li, M., et al. (2019). Element replacement approach by reaction with Lewis acidic molten salts to synthesize MXenes. *Journal of the American Chemical Society, 141*(11), 4730–4737.
[10] Xia, X., Zhang, P., Nie, F., Liang, J., Zhang, C., Maitlo, I., Lou, H., Shen, C., Ding, J., et al. (2026). In situ growth of Sn nanowires on an Al matrix using Ti_2SnC as a Sn source. *Nanoscale*. DOI: 10.1039/d6nr00521g.
[11] Zhang, Z., et al. (2015). Origin of Al deficient Ti_2AlN and pathways of vacancy-assisted diffusion. *The Journal of Physical Chemistry C, 119*(29), 16606–16613.
[12] VahidMohammadi, A., Rosen, J., & Gogotsi, Y. (2021). The world of two-dimensional carbides and nitrides (MXenes). *Science, 372*(6547), eabf1581.
[13] Wyatt, B. C., et al. (2022). MXene synthesis from MAX phase precursors and the role of etching chemistry. *Nature Synthesis, 1*, 587-598.

DOI: 10.54254/2755-2721/2026.36441

[14] Zhang, C. J., et al. (2020). Oxidation stability and surface chemistry of $Ti_3C_2T_x$ MXene. *Advanced Functional Materials, 30*(47), 2000714.
[15] Wang, L., et al. (2023). Direct synthesis of two-dimensional MXenes. *Science, 379*(6638), 1242-1247.
[16] Hassan, T., et al. (2026). Quantitative defect–property correlations in Ti_3C_2Tx MXenes via precursor-controlled defect engineering. *Nano-Micro Letters, 18*, 216.
[17] Lu, Y., et al. (2021). Isotope study reveals atomic motion mechanism for the formation of metal whiskers in MAX phases. *Acta Materialia, 204*, 116524.
[18] Kruger, D. D., et al. (2024). Molten salt derived MXenes: Synthesis and applications. *Advanced Science, 11*, 2307106.
[19] Zhang, Q., et al. (2022). Rapid and massive growth of tin whisker on mechanochemically decomposed Ti_2SnC. *Materials Today Communications, 31*, 103483.
[20] Liu, Y., et al. (2023). Mitigation of metal whisker growth from MAX phases by A-site alloying. *Applied Surface Science, 631*, 157539.
[21] Xu, L., et al. (2006). Growth of intermetallic layer in multi-laminated Ti/Al diffusion couples. *Materials Science and Engineering A, 435–436*, 638-647.